Protoplasma (1994) 182: 39 – 52

PROTOPLASMA

Nucellar projection transfer cells in the developing wheat grain

H. L. Wang, C. E. Offler*, and J. W. Patrick

Department of Biological Sciences, The University of Newcastle, Newcastle, New South Wales

Received January 21, 1994
Accepted May 16, 1994

Summary. Transfer cells in the nucellar projection of wheat grains at 25 ± 3 days after anthesis have been examined using light and electron microscopy. Within the nucellar tissue, a sequential increase in non-polarized wall ingrowth differentiation and cytoplasmic density was evident. Cells located near the pigment strand were the least differentiated. The degree of differentiation increased progressively in cells further removed from the pigment strand and the cells bordering the endosperm cavity had degenerated. Four stages of transfer cell development were identified at the light microscope level. Wall ingrowth differentiation followed a sequence from a papillate form through increased branching (antler-shaped ingrowths) which ultimately anastomosed to form a complex labyrinth. The final stage of wall ingrowth differentiation was compression which resulted in massive ingrowths. In parallel with wall ingrowth deposition cytoplasmic density increased. During wall deposition, paramural and multivesicular bodies were prominent and were in close association with the wall ingrowths. The degeneration phase involved infilling of cytoplasmic islets within the wall ingrowths. This was accompanied by complete loss of the protoplast. The significance of this transfer cell development for sucrose efflux to the endosperm cavity was assessed by computing potential sucrose fluxes across the plasma membrane surface areas of the nucellar projection cells. Transfer cell development amplified the total plasma membrane surface area by 22 fold. The potential sucrose flux, when compared with maximal rates of facilitated membrane transport of sugars, indicated spare capacity for sucrose efflux to the endosperm cavity. Indeed, when the total flux was partitioned between the nucellar projection cells at the three stages of transfer cell development, the fully differentiated stage III cells located proximally to the endosperm cavity alone exhibited spare transport capacity. Stage II cells could accommodate the total rate of sucrose transfer, but stage I cells could not. It is concluded that the nucellar projection tissue of wheat provides a unique opportunity to study transfer cell development and the functional role of these cells in supporting sucrose transport.

Keywords: Nucellar projection; Symplast/apoplast sucrose exchange; Transfer cell; Wall ingrowth development; Wheat grain.

* Correspondence and reprints: Department of Biological Sciences, The University of Newcastle, Newcastle, NSW 2308, Australia.

Abbreviations: CSPMSA cross sectional plasma membrane surface area; LPMSA longitudinal plasma membrane surface area; PTS trisodium 3-hydroxy-5,8,10-pyrenetrisulfonate.

Introduction

Transfer cells develop from many types of differentiated plant cells and are found in a variety of different plant organs (Pate and Gunning 1972). They are characterized by convoluted wall ingrowths and, as a consequence, amplification of their plasma membrane surface areas. It is generally accepted that this membrane amplification (3 to 20 fold; Bonnemain et al. 1991) facilitates apoplast/symplast solute exchange. Further, there is an increasing body of evidence that underscores the significant role of transfer cells in solute transport (e.g., Gunning and Pate 1974, Jones and Dropkin 1976, Gunning 1977, Newcomb and Peterson 1979, Landsberg 1986, Wimmers and Turgeon 1991, Offler and Patrick 1993, Wang et al. 1994 a).

Transfer cells occur in tissues responsible for high solute fluxes (Pate and Gunning 1972). This could well account for the changes in the cellular location of transfer cells during seed development, for example, in developing seed of *Vicia faba* (Pate and Gunning 1972). In this and other species, differentiation of transfer cells is most evident at the maternal/embryonic interface. Thus, early in seed development, the suspensor of *Phaseolus* and the cellular endosperm facing the perisperm of *Mesembryanthemum* differentiate into transfer cells (Pate and Gunning 1972). During the phase of rapid dry matter accumulation, transfer cells commonly occur at the seed coat/cotyledon interface in seed of the grain legume *V. faba* (Offler et al. 1989), the pericarp/

aleurone interface in *Sorghum* caryopses (Maness and McBee 1986), yellow foxtail (Rost and Lersten 1970), and millet (Zee and O'Brien 1971), and the pericarp/endosperm interface in maize kernels (Felker and Shannon 1980, Davis et al. 1990). Their importance during this phase of seed growth has yet to be established unequivocally. However, in the case of *V. faba* there is correlative evidence linking transfer cell development and enhanced cotyledon growth rate (Bonnemain et al. 1991) and, for the seed coat transfer cells, quantitative structural studies (Offler and Patrick 1993) indicate that they are the principal cellular site for membrane transfer of sucrose to the seed apoplast.

In the developing grain of wheat and barley, the nucellar cells of the crease region of the grain pericarp project into the endosperm cavity. This so-called nucellar projection is located between the maternal and filial tissues (Cochrane 1983) and forms the terminus for short-distance transfer of solutes within the maternal pericarp tissues (Wang et al. 1994 a). The nucellar projection cells differentiate into transfer cells during the filling phase of grain growth (Cochrane and Duffus 1980, Cochrane 1983, Wang et al. 1994 a). By quantifying the plasma membrane surface area of these cells, we have demonstrated that their capacity for membrane exchange is commensurate with the dry weight gain of the grain (Wang et al. 1994 a). Some structural features of the nucellar projection transfer cells have been described by Cochrane and Duffus (1980) for barley. However, the account by these authors is limited to comment on wall ingrowth morphology and there is no equivalent statement for the nucellar projection cells of wheat. This deficiency in our knowledge of the structural characteristics of these specialized cells can be attributed, at least in part, to technical difficulties encountered in establishing fixation and staining procedures that permit all features of the cell ultrastructure to be resolved.

The purpose of this paper is to describe the development of nucellar projection transfer cells and to relate the stage of development of these cells to their capacity for plasma membrane efflux of sucrose. Grains at 25 ± 3 days after anthesis were selected for study since this is the mid-stage of the linear phase of grain filling (Sofield et al. 1977) when grain dry weight gain is most rapid.

Materials and methods

Plant material

Wheat plants (*Triticum turgidum* var. *durum* cv. Fransawi) were grown in pots under glasshouse conditions for one month and thereafter in a controlled environment growth cabinet as described previously (Wang et al. 1993). Mineral nutrients were supplied as a 10 g/m^3 solution of Aquasol (Hortico Aust. Ltd, Sydney) at the rate of 0.5 cm^3 per plant per week. Plants were trimmed to a single primary tiller and the anthesis date for each ear was recorded.

Grains were selected for experiments from the "a" floret position (Bremner and Rawson 1978) of spikelets located in the mid-region of the ears at 25 ± 3 d after anthesis.

Light and transmission electron microscopy

Transverse slices, 1 mm in thickness, were cut from the middle of 3 grains harvested from each of 3 plants and fixed using one of the two procedures detailed below.

(a) Tissue slices were fixed in 2.5% glutaraldehyde and 2.5% paraformaldehyde in 50 mM cacodylate buffer at pH 7.0 at 0 °C for 5 h. Following five 15 min washes in 50 mM cacodylate buffer, tissue was post fixed with 1% osmium tetroxide in distilled water for 3 h at 0 °C. After five 15 min washes in distilled water, the tissue was treated with 1% tannic acid for 2 h at room temperature (method modified from Park et al. 1982). This method was used to improve the contrast of sections from Spurrs-embedded tissue to visualize cytoplasmic contents.

(b) Tissue slices were fixed with 2.5% glutaraldehyde, 2.5% paraformaldehyde and 2% tannic acid in 25 mM phosphate buffer at pH 7.0 for 2 h at 0 °C. Tissue was washed in five 15 min changes of 25 mM phosphate buffer before being post fixed with 2% $FeCl_3$ for 2 h at room temperature (method modified from Overall et al. 1982). This procedure enhanced the visibility of wall structure.

At the completion of post fixation, tissue slices were washed twice for 15 min each in either 50 mM cacodylate (a) or 25 mM phosphate (b) buffer and stored overnight in buffer at 0 °C. Following another two 15 min rinses in buffer, the fixed tissue was dehydrated through a 10% step-graded acetone series at 0 °C and infiltrated over 2 days through a five-step graded series from 100% acetone to 100% Spurr's epoxy resin (Spurr 1969) and a further 7 days in 100% resin. Blocks were polymerised by exposure to a temperature sequence of 37 °C for 12 h, 48 °C for 12 h, and 70 °C for 24 h over a period of 48 h.

Semithin sections, 1–2 µm thick, were cut with glass knives using a Reichert-Jung Ultracut E, stained with 0.5% toluidine blue in sodium

Fig. 1 A, B. Light micrographs illustrating the nucellar projection of the developing wheat grain at 25 ± 3 days after anthesis. Bars: 50 µm. **A** Transverse section of the nucellar projection showing the sequence of progressive development and degeneration of nucellar projection transfer cells from those cells contiguous with the pigment strand to those adjacent to the endosperm cavity. Four developmental stages based on wall thickness and cytoplasmic density are identified as stages I, II, III, and IV. The cells at each stage of development are delineated between the arrows. **B** Longitudinal section of the nucellar projection with transfer cells at the four developmental stages delineated by arrows. *Cu* Cuticular layer; *Ec* endosperm cavity; *El* empty lumen; *Dc* dense cytoplasm; *Ne* nucellar epidermal cells; *Np* nucellar projection; *Ps* pigment strand; *S I* developmental stage I; *S II* stage II; *S III* stage III; *S IV* stage IV

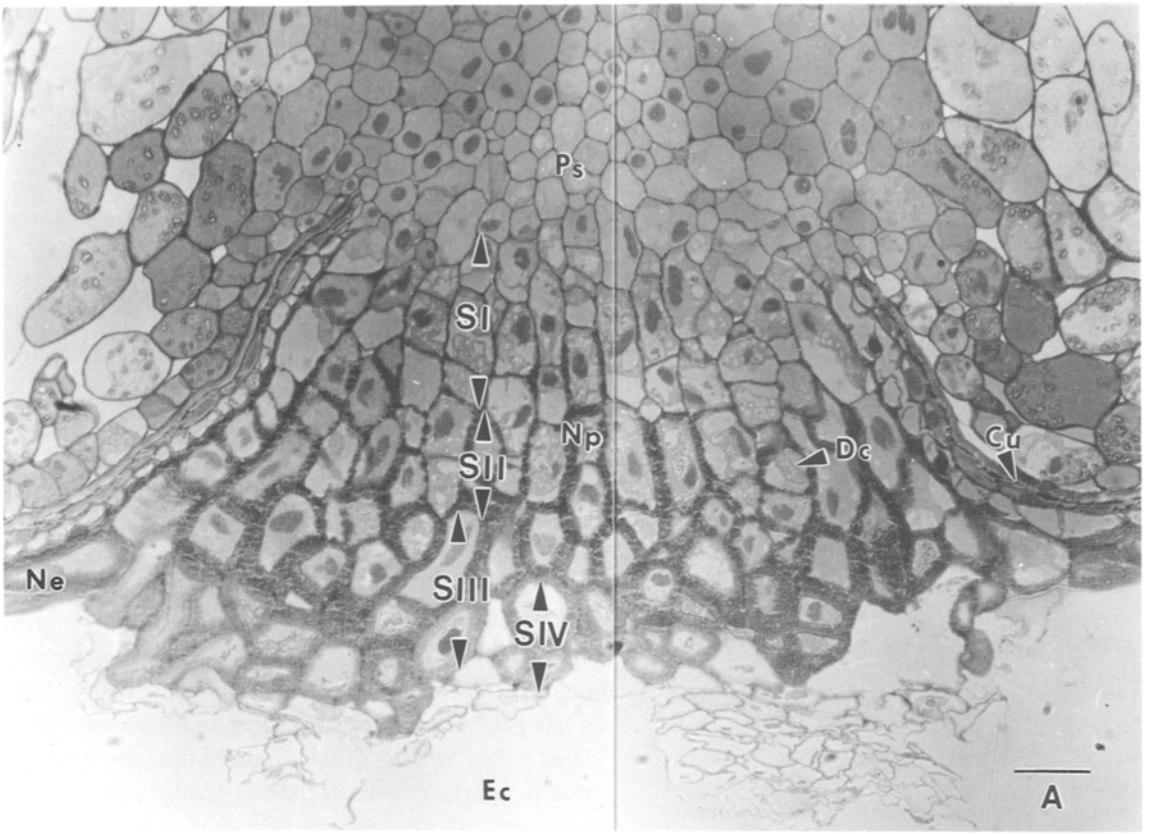
Ps
SI
SII
SIII
SIV
Np
Dc
Cu
Ne
Ec
A

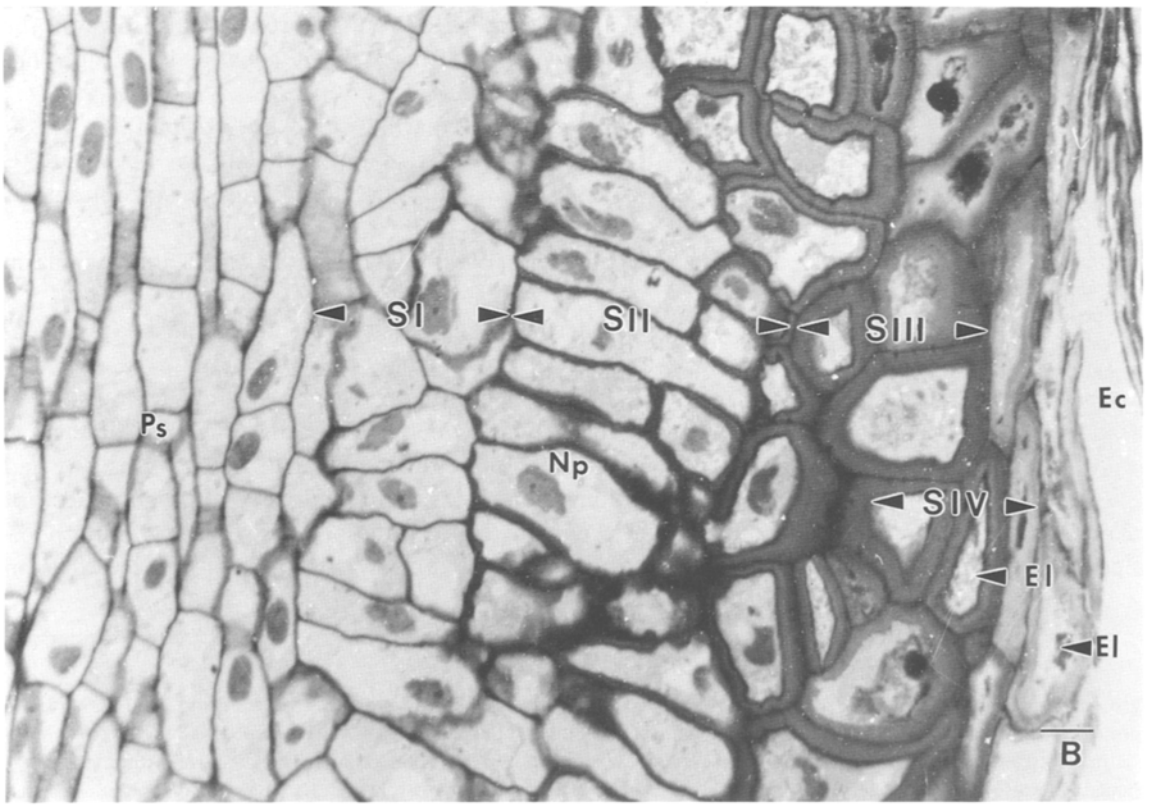
SI
SII
SIII
Ps
Np
Ec
SIV
EI
EI
B

carbonate buffered to pH 9, and examined with a Zeiss Axiophot photomicroscope.

Ultrathin sections, 60 nm thick, were cut with a diamond knife, stained with potassium permanganate and lead citrate (Bray and Wagener 1978) and observed in either a Jeol JEM-100 CX or Jeol JEM-1200 EX II electron microscope.

Plasma membrane amplification, plasma membrane surface area, and estimated sucrose flux

The plasma membrane amplification resulting from wall ingrowth formation at stages I to III of development of the nucellar projection transfer cells was calculated from the extended length of plasma membrane in the vicinity of wall ingrowths and the length of the corresponding secondary cell wall. This was done from electron micrographs cut from 3 grains using a chartometer. Fourteen cells were scored for stages I and III and 11 cells for stage II.

The plasma membrane surface area was obtained by summing the longitudinal and cross sectional surface areas (LPMSA and CSPMSA, respectively). In addition, an hypothetical estimate was made excluding the contribution resulting from the formation of wall ingrowths. LPMSA and CSPMSA per grain were estimated separately for cells at stages I to III of transfer cell development and for the nucellar epidermal cells (Fig. 1 A). These estimates were obtained from light and electron micrographs of longitudinal and transverse sections. LPMSA was obtained by multiplying transfer cell plasma membrane perimeter in transverse section [cell perimeter (cm) with wall ingrowths × appropriate amplification factor + cell perimeter without wall ingrowths (if applicable)] to the amplified length in longitudinal section [crease tissue length (cm) × appropriate amplification factor × the proportion of cell length with wall ingrowths + crease length without wall ingrowths (if applicable)]. CSPMSA was estimated by doubling the surface area of a transverse section of the appropriate cells to allow for two end walls per cell and multiplying this figure by the number of cells along the length of the grain. (A weight ratio method was used to obtain the surface area and the number of cells along the length of the grain was estimated from the length of the crease region and mean cell length.) Potential fluxes (mol/m^2/s) for plasma membrane exchange of sucrose were computed using the observed rate of sucrose delivery of 55×10^{-12} mol/s/grain (Wang et al. 1993) and the estimated plasma membrane surface areas of the nucellar projection cells at stages I to III of transfer cell development and of the nucellar epidermal cells. These potential fluxes of sucrose were compared with values for maximal fluxes for facilitated membrane transport of sugars ($1–10 \times 10^{-8}$ mol/m^2/s; see Lüttge and Higinbotham 1979).

Results

In grain at 25 ± 3 days after anthesis, the nucellar projection is composed of 8–10 rows of cells which project into the endosperm cavity (Fig. 1). These cells are separated from the crease vascular bundle by the pigment strand which forms a bridge between the ends of the cuticularized epidermis of the pericarp (Fig. 1 A) and a barrier to transfer within the apoplast (Wang et al. 1994 b). Non-polarized wall ingrowth differentiation had occurred in most of the nucellar projection cells of grains at 25 ± 3 days after anthesis. This is consistent with the observation that wall ingrowth development commences in the nucellar projection cells between 7 and 9 days after anthesis and by 19 days after anthesis most cells have wall ingrowths (Irwanto and Offler unpubl. data). Examination of transverse (Fig. 1 A) and longitudinal (Fig. 1 B) sections reveals a sequential increase in wall differentiation and cytoplasmic density followed by degeneration of the cytoplasm. Cells located near the pigment strand appear to be the least differentiated and those adjacent to the endosperm cavity appear devoid of cytoplasm (Fig. 1 A, B). A similar sequence of deposition of wall material to form transfer cell wall ingrowths has been reported for the basal endosperm of the maize kernel (Davis et al. 1990). The differentiation of wall ingrowths, which is the basis for classifying these nucellar projection cells as transfer cells (Gunning and Pate 1972), appears to occur as a continuum. However, the following four stages can be identified at a light microscope level (Fig. 1).

Stage I: Walls partially thickened (pitted) and cytoplasm organelle-rich and vacuolated.

Stage II: Walls darkly stained, thick and cytoplasm less vacuolated.

Stage III: Walls massively thickened and cytoplasm dense with small vacuoles.

Stage IV: Walls massively thickened and cytoplasm absent leaving an empty cell lumen.

In each of these four recognised stages of transfer cell differentiation/degeneration the thickness of the cell wall was found to be equivalent in both transverse and longitudinal section (cf. Fig. 1 A, B). The pattern of progressive differentiation of wall ingrowth morphology is presented below, together with observations on

Fig. 2 A–C. Electron micrographs of the nucellar projection showing predominantly developmental stage I transfer cells. **A** Transverse section of the nucellar projection transfer cells located adjacent to the pigment strand. Note the papillate and antler-shaped wall ingrowths and pit-fields of plasmodesmata (arrows) interconnecting the transfer cells. Bar: 3.0 µm. **B** and **C** Parts of nucellar projection cells illustrating papillate (**B**) and antler-shaped (**C**) wall ingrowths. Asterisks pinpoint vesicles adjacent to the wall ingrowths and in **C** arrows pinpoint plasmodesmata. Bars: 0.5 µm. Tissue was fixed in glutaraldehyde/paraformaldehyde/tannic acid and post-fixed with ferric chloride (see Materials and methods). *Awi* Antler-shaped wall ingrowths; *Iwi* ingrowth wall parallel to the original secondary wall; *Nu* nucleus; *Pwi* papillate wall ingrowths; *Rer* rough endoplasmic reticulum; *S I* developmental stage I; *S II* stage II; *Va* vacuole

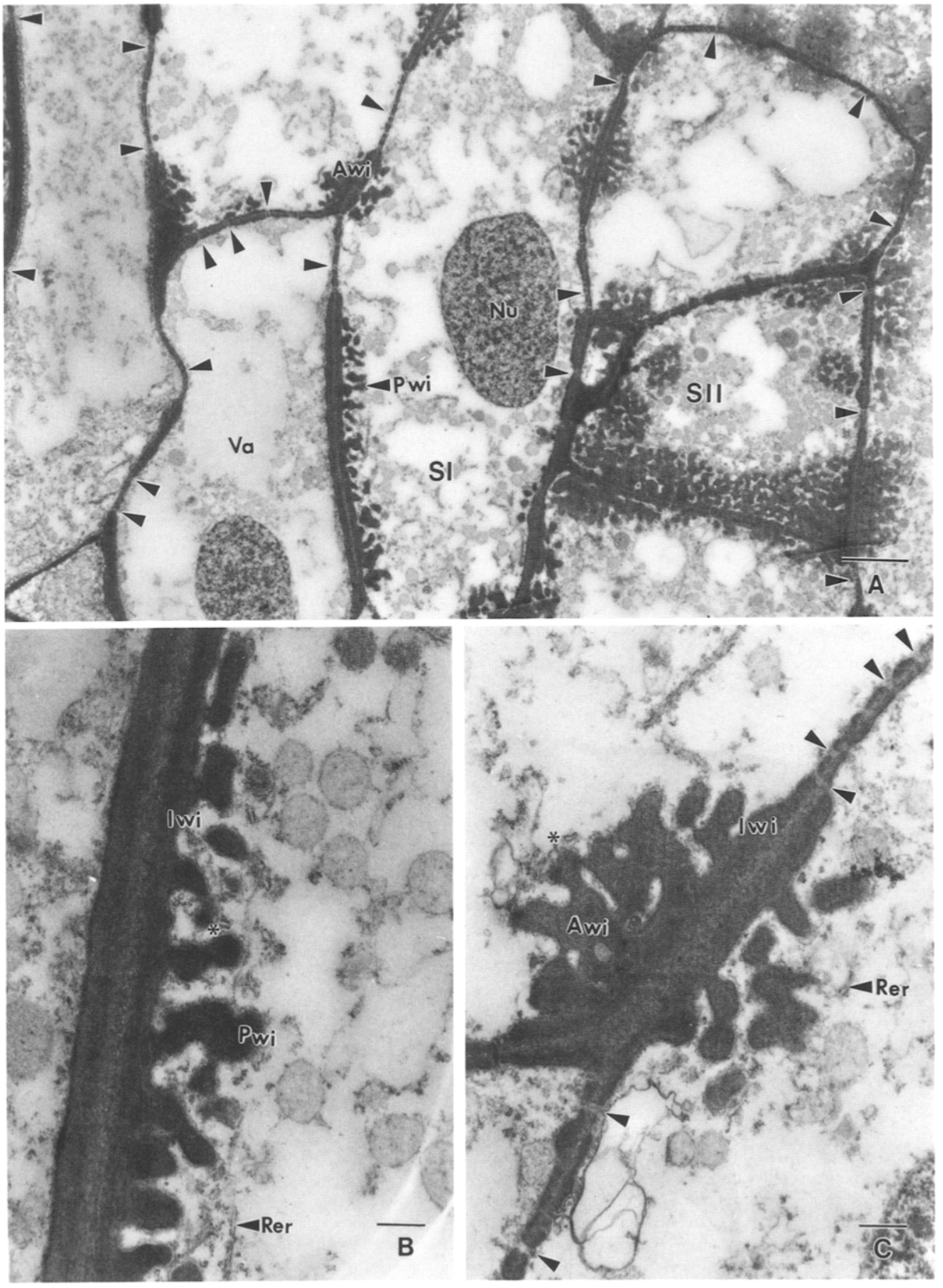
Awi
Nu
Pwi
SII
Va
SI
A
Iwi
*
Pwi
Rer
B
Iwi
*
Awi
Rer
C

cytoplasmic features and, in particular, those relevant to transfer cell transport function.

Wall ingrowth morphology

Stage I

In cells at stage I, ingrowths were restricted to lengths of wall separating primary pit-fields of plasmodesmata and where the walls of three cells join (Fig. 2 A, C). This pattern of initial deposition of wall ingrowths was responsible for the uneven thickness of cell walls observed under light microscopy (Fig. 1 A). Ingrowth development appeared to commence with deposition of a band of more densely staining wall material laid down parallel to the original secondary wall (Fig. 2 B, C). This remained evident at least until stage II (Fig. 3 C, D) and sometimes for longer depending on the degree of ingrowth compression. In some cells, the only additional secondary wall development was this parallel band (Fig. 2 B) while in adjacent cells wall ingrowths arising from this band were papillate or antler-shaped at the first stage of transfer cell development (Fig. 2 A–C). The latter wall deposition resulted in a 3.84 fold amplification of their plasma membranes (Table 1). Of the total number of nucellar projection cells, approximately 21% were at stage I of development in grain at 25 ± 3 days after anthesis (Table 1).

Stage II

Cells at developmental stage II had more extensive ingrowths which formed a complex branched and anastomosing labyrinth (Pate and Gunning 1972) in both longitudinal (Fig. 3 C) and transverse (Fig. 3 D) sections. In some contiguous cells, extensive wall ingrowths were evident on one side of a common wall while only small ingrowths (stage I) arose from the other side (Fig. 3 A, B). At stage II, wall ingrowth formation was responsible for a 6 fold amplification of the plasma membrane but only 14% of the nucellar projection cells were at this stage of development (Table 1). The wall ingrowths of both stage I and stage II were more darkly stained than the original secondary wall (Figs. 2 B, C and 3 D).

Stage III

By stage III a massive wall ingrowth akin to flange-shaped ingrowths (Pate and Gunning 1972) had formed by fusion of the complex labyrinth (Figs. 3 B and 4). The inner border of the ingrowth wall remained irregularly and deeply lobed and resembled the microvilli of epithelial cells (Tripathi and Boulpaep 1989). The entire cell wall exhibited this type of ingrowth in which islets of cytoplasm were evident (Fig. 4 B, C). The somewhat flange-shaped appearance resulted from the uneven distribution of the cytoplasmic islets within the wall (Figs. 4 B and 5 A). At this stage of the development of the ingrowths, the cell wall microfibrillar organization was clearly discernable (Fig. 4 C). Microfibrils were loosely packed and their orientation followed the contours of the ingrowths (Fig. 4 C). This organization of microfibrils has been recognised in the ingrowths of the thin-walled parenchyma transfer cells of the seed coat of *V. faba* (Offler and Patrick 1993) and may well be a common feature of ingrowth deposition. The nucellar projection transfer cells exhibiting this ingrowth morphology were considered to be fully differentiated (Figs. 3 B, 4 A, B, and 5 A, B). They have an amplification of 6.9 and constituted nearly 50% of the cells in the grain examined (Table 1).

Stage IV

The cells bordering the endosperm cavity had degenerated (Fig. 1). These cells retained the massively thickened wall of viable, fully developed transfer cells. However, in contrast to cells at stage III, their entire wall ingrowth labyrinth was compressed and infilled, apparently by wall material (Figs. 5 B and 6 A). The extent

Fig. 3 A–D. Electron micrographs to illustrate the nucellar projection cells at developmental stage II. Bars: A and B, 0.3 μm; C and D, 0.5 μm. **A** Transverse section of a stage II transfer cell located adjacent to cells at stage I. Note that the wall ingrowths change from papillate and antler-shaped to a complex branched and anastomosing labyrinth. Pit-fields of plasmodesmata are indicated by arrows. **B** Transverse section of stage II transfer cells adjoining cells which have developed to stage III. Note that the wall ingrowth changes from the complex branched and anastomosing labyrinth to a massive wall ingrowth akin to flanges in stage III (the latter indicated by asterisks). Pit-fields of plasmodesmata are indicated by arrows. **C** and **D** Parts of the complex branched and anastomosing wall ingrowth labyrinth in longitudinal (**C**) and transverse (**D**) section. Arrows indicate plasmodesmata. Note paramural bodies and short lengths of rough endoplasmic reticulum adjacent to, or fused with, the plasma membrane of wall ingrowths (asterisks). Tissue was fixed in glutaraldehyde/paraformaldehyde/tannic acid and post-fixed with ferric chloride (see Materials and methods). *Awi* Antler-shaped wall ingrowths; *Iwi* ingrowth wall parallel to the original secondary wall; *Lwi* wall ingrowth labyrinth; *Mwi* massive wall ingrowths; *Nu* nucleus; *Pa* paramural body; *Rer* rough endoplasmic reticulum; *S I* developmental stage I; *S II* stage II; *S III* stage III; *Va* vacuole

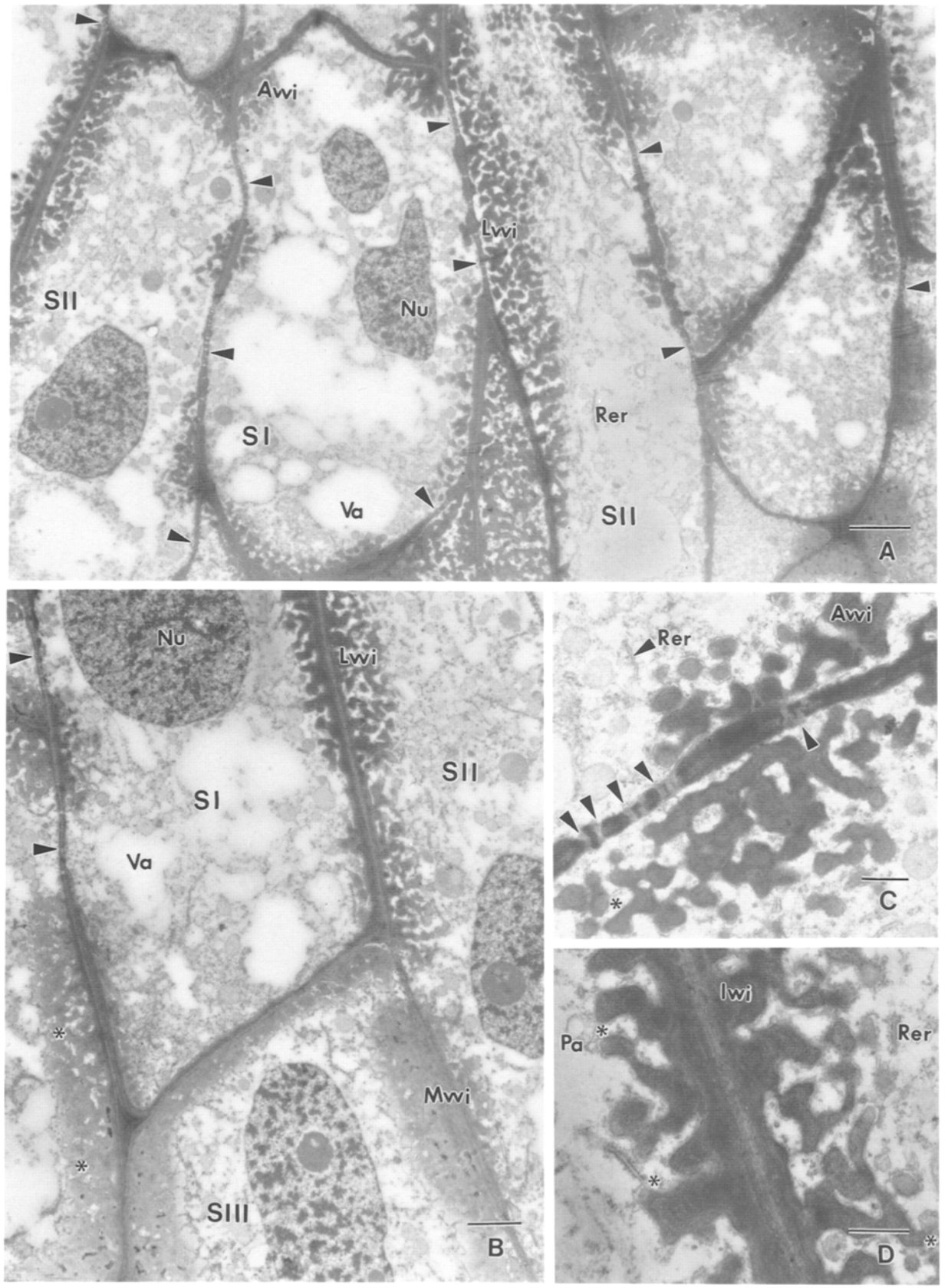
Awi
Lwi
Nu
SII
SI
Va
Rer
SII
A
Nu
Lwi
SII
SI
Va
Mwi
SIII
B
Rer
Awi
C
Iwi
Pa
Rer
D

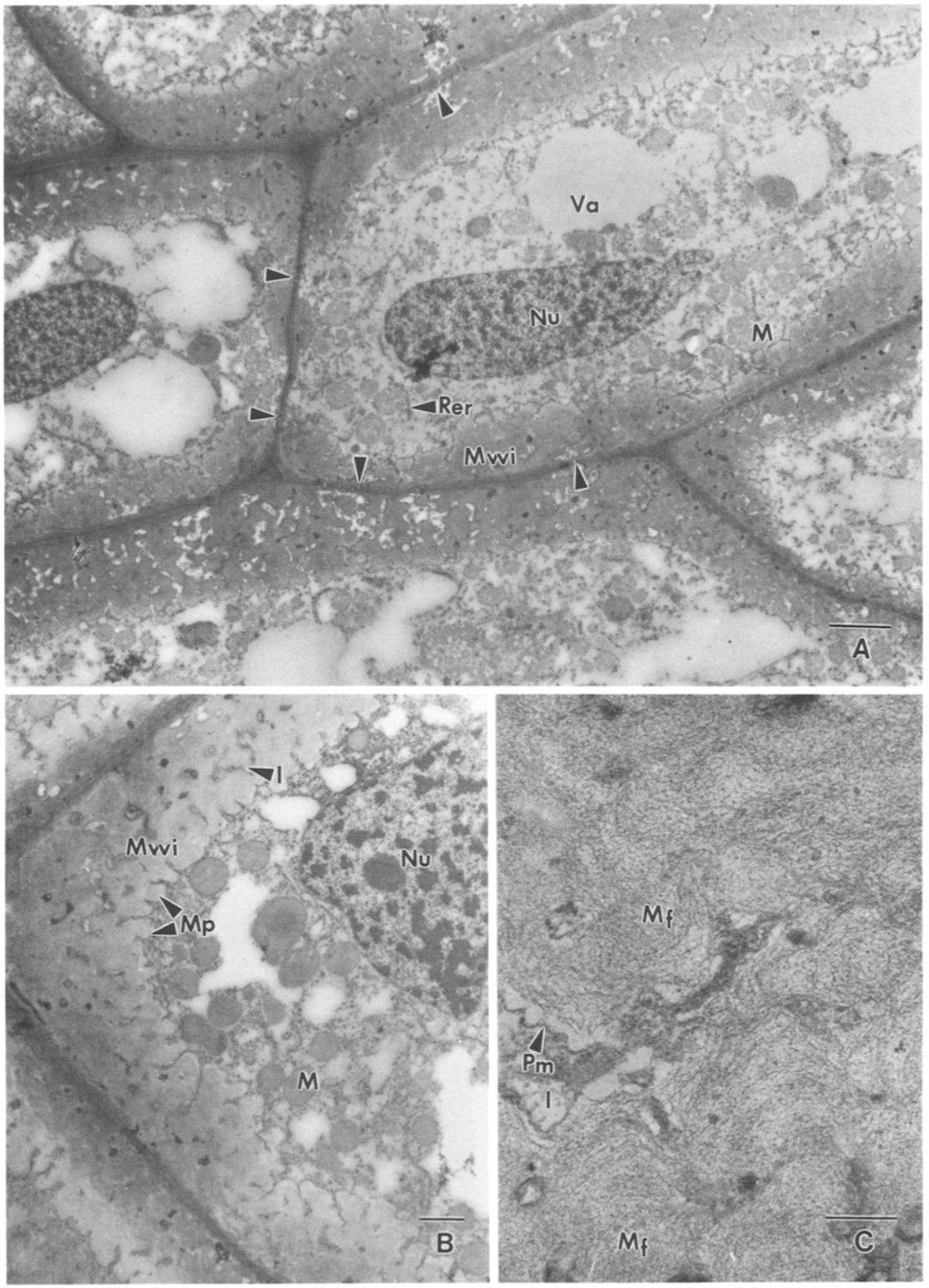

Fig. 4 A–C. Electron micrographs of transverse sections of fully differentiated nucellar projection transfer cells (stage III) located adjacent to cells at stage II. Bars: A and C, 2 μm; B, 1.0 μm. **A** Section of several cells showing the massive wall ingrowths with microvilli-like projections at their inner border. The cytoplasm is dense with abundant mitochondria and an extensive rough endoplasmic reticulum network. Pit-fields of plasmodesmata are indicated by arrows. **B** Portion of a cell showing the islets of cytoplasm formed by compression of the wall ingrowth labyrinth and the microvilli-like projections at the inner border of the massive ingrowths. **C** High magnification micrograph of part of the wall ingrowths showing the loosely packed microfibrils. Tissue was fixed in glutaraldehyde/paraformaldehyde/tannic acid and post-fixed with ferric chloride (see Materials and methods). *I* Islet of cytoplasm; *M* mitochondrion; *Mf* microfibrils; *Mp* microvilli-like projections; *Mwi* massive wall ingrowth; *Nu* nucleus; *Pm* plasma membrane; *Rer* rough endoplasmic reticulum; *Va* vacuole

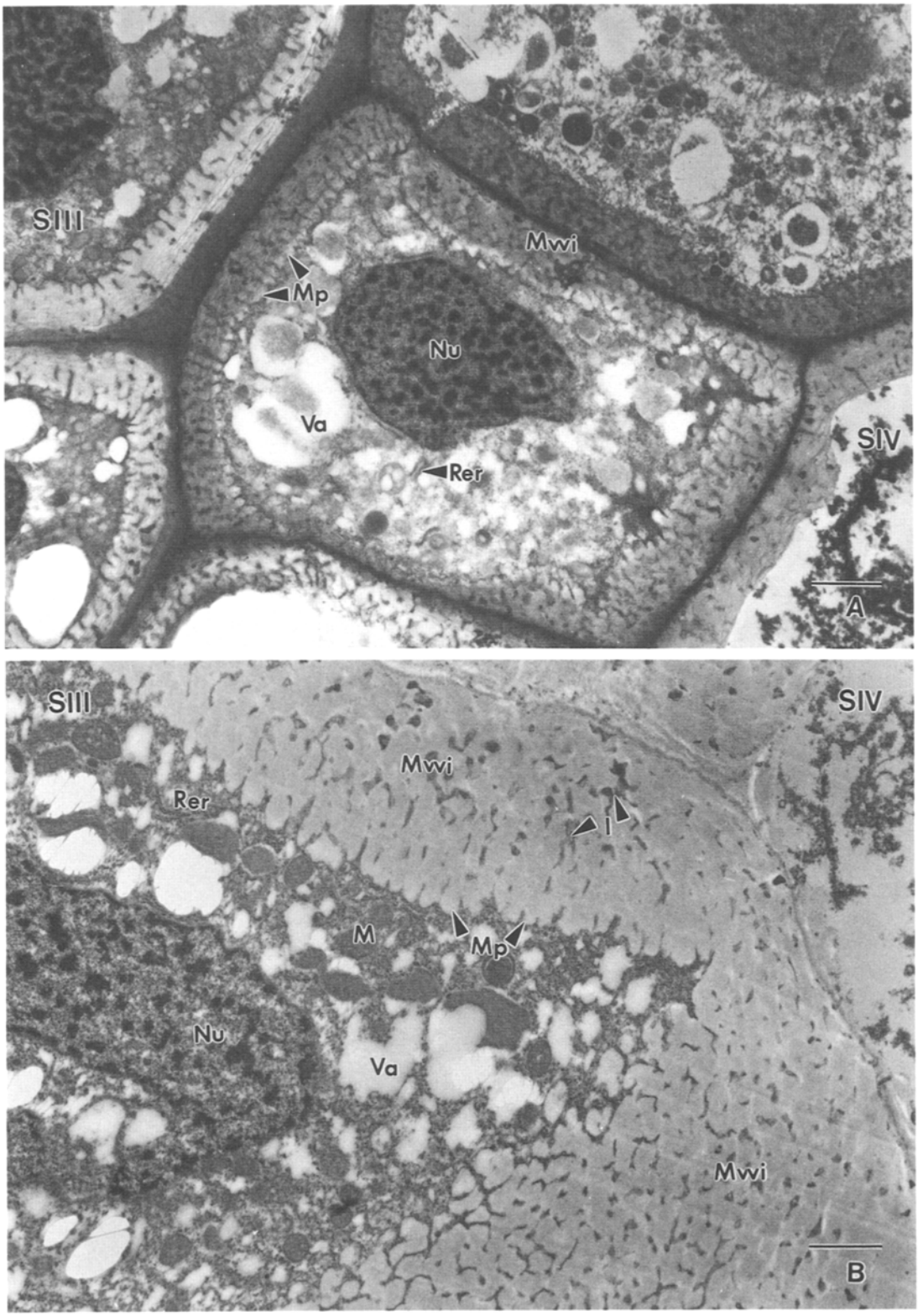

Fig. 5 A, B. Electron micrographs of transverse sections of fully differentiated nucellar projection transfer cells (stage III) located adjacent to cells at stage IV. Bars: 0.1 µm. **A** A cell adjoined by stage III and stage IV transfer cells. Note the massive wall ingrowths and the dense cytoplasm and prominent nucleus. **B** Part of a cell illustrating the massive wall ingrowths with microvilli-like projections at their inner border and islets of cytoplasm. Note the dense cytoplasm characterized by smaller vacuoles and increased numbers of mitochondria relative to those in cells at stages I and II (Figs. 2 A and 3 A, respectively). Tissue was fixed in glutaraldehyde/paraformaldehyde/tannic acid and post-fixed with ferric chloride (see Materials and methods). *I* Islet of cytoplasm; *M* mitochondrion; *Mp* microvilli-like projections; *Mwi* massive wall ingrowth; *Nu* nucleus; *Rer* rough endoplasmic reticulum; *S III* developmental stage III; *S IV* stage IV; *Va* vacuole

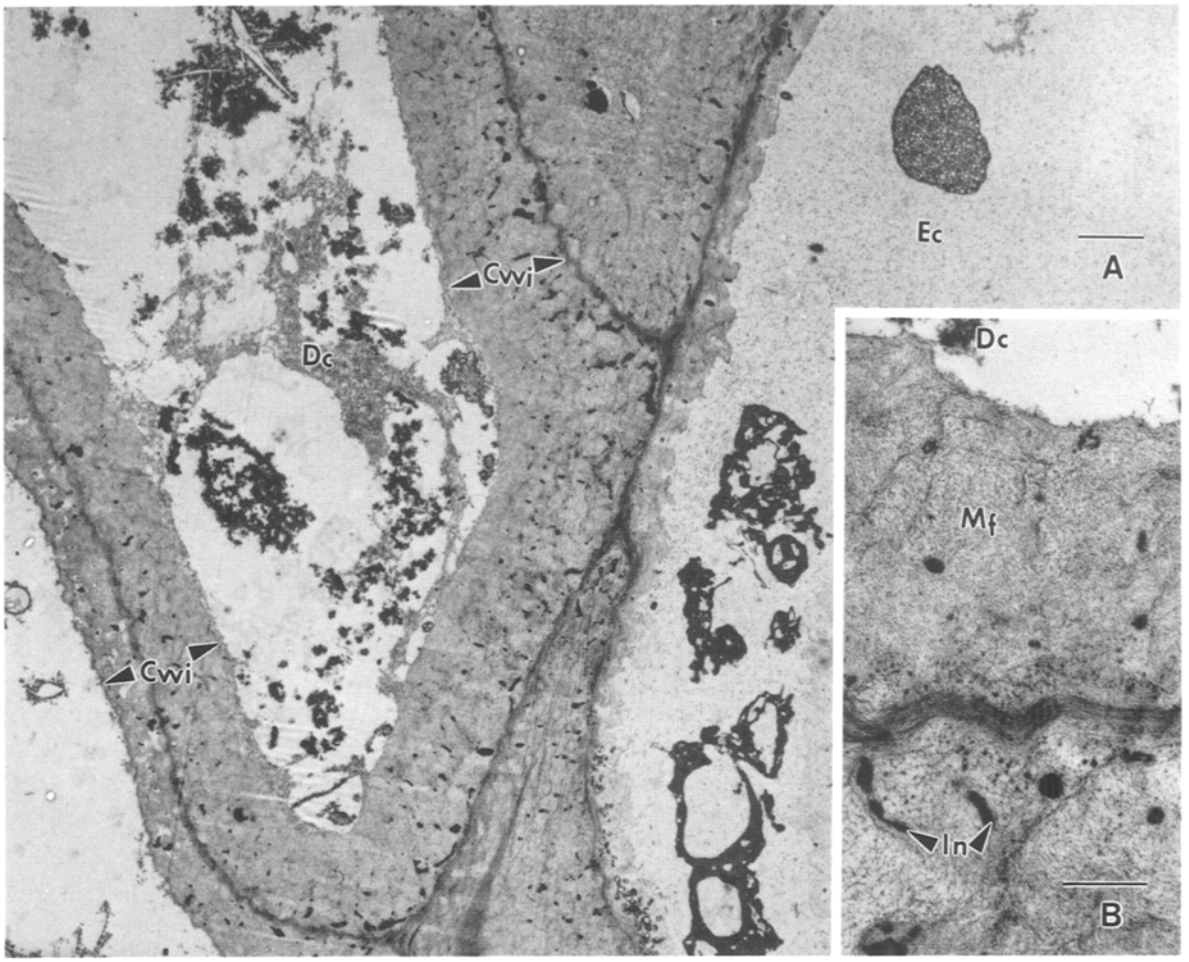

Fig. 6 A, B. Electron micrographs of **A** a longitudinal section of part of a stage IV nucellar projection transfer cell and **B** an enlargement of part of the wall ingrowth. Note that the entire wall ingrowth labyrinth is compressed and the cytoplasm has degenerated. No plasma membrane is evident and the cytoplasmic islets are infilled. Bar: for A, 2.0 μm; for B, 0.5 μm. Tissue was fixed in glutaraldehyde/paraformaldehyde/tannic acid and post-fixed with ferric chloride (see Materials and methods). *Cwi* Compressed wall ingrowths; *Dc* degenerated cytoplasm; *Ec* endosperm cavity; *In* infilled islet; *Mf* microfibrils

to which this infilling had occurred differed between cells (Fig. 5 A and cf. Figs. 5 B and 6 A). One or two rows of these degenerated cells formed the inner border of the nucellar projection tissue (Fig. 1) and accounted for 18% of the total number of cells. These degenerated cells were classified as stage IV.

Cytoplasmic characteristics

The transfer cells exhibited an organelle rich, dense cytoplasm at stages I to III of differentiation (Figs. 2–5). In general, they were characterized by a prominent nucleus, abundant mitochondria, small lengths of rough endoplasmic reticulum, polyribosomes, vesicles and vacuoles of varying size. An overall increase in cytoplasmic density occurred with differentiation (Fig. 2A; cf. Fig 4 A) which was mainly attributable to a decrease in vacuolation (Figs. 2–5). In stage I cells, the rough endoplasmic reticulum was more obvious than at the other two stages. Here both long and short lengths of endoplasmic reticulum occurred in close association with the wall ingrowths (Fig. 7 A) and in some cells the rough endoplasmic reticulum was found touching or fused with the plasma membrane of the wall ingrowths (Fig. 3 C, D). In their studies on the differentiating tracheary elements in developing leaves of sugar beet, Esau et al. (1966) found that the endoplasmic reticulum is associated with the plasma membrane. These and other authors (e.g., Chrispeels 1980) suggest that the rough endoplasmic reticulum may be involved in cell wall deposition. Paramural bodies and groups of small vesicles, "multivesicular bodies" (Marchant and Robards 1968) were prominent in cells at

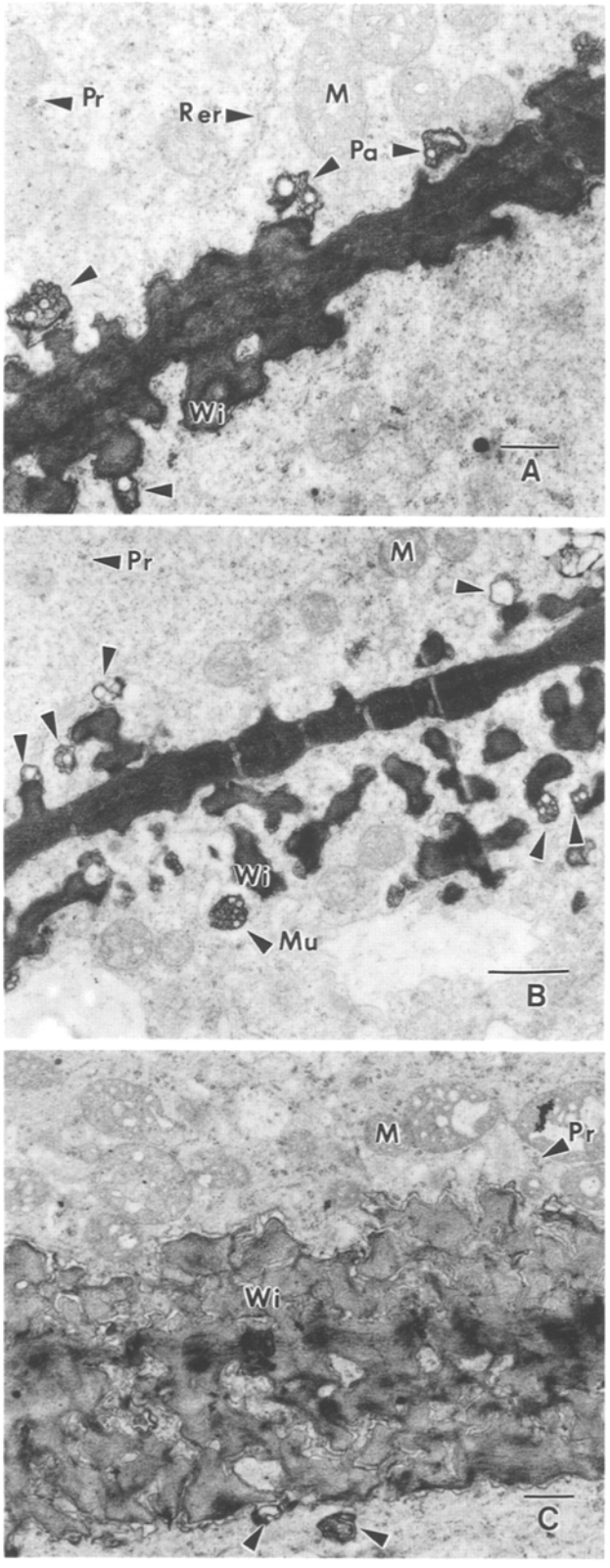

stages I and II of differentiation (Figs. 3 D and 7 A, B) where they were found in association with the wall ingrowths. While some of these bodies were also observed in stage III cells (Fig. 7 C), they were less conspicuous. Given the existance of the multivesicular bodies, the paramural bodies can be classified as lomasomes (see Marchant and Robard 1968). By stage IV the cytoplasm had partially or completely degenerated, in the latter case leaving an empty lumen (Figs. 1 and 6) and no plasma membrane (Fig. 6 B).

Potential membrane fluxes of sucrose

Previous studies using the apoplastic tracers PTS and Calcofluor white (Wang et al. 1994 b) have established continuity between the apoplast of the nucellar projection and the endosperm cavity. Given this, it can be assumed that all the nucellar projection cells have the potential to contribute to plasma membrane exchange of sucrose to the endosperm cavity. Therefore, the potential sucrose flux across the combined plasma membrane surface areas of cells of stages I to III and the nucellar epidermal cells has been computed using the observed rate of sucrose transport to the starchy endosperm. In addition, a hypothetical flux estimate has been made excluding the contribution to plasma membrane surface area resulting from wall ingrowth development. Both flux values are presented in Table 1. When compared with values for maximal fluxes for facilitated membrane transport of sugars (i.e., 1–10×10^{-8} mol/m^2/s; Lüttge and Higinbotham 1979), the potential flux in the absence of wall ingrowth development was 5 fold higher than the reported maximum (Table 1). However, when the amplified plasma membrane surface area was used (Table 1), the potential flux fell within the reported range (Table 1). This latter flux value indicates that the nucellar projection transfer cells have spare capacity for plasma membrane exchange of sucrose to the endosperm cavity for ac-

Fig. 7 A–C. Electron micrographs of longitudinal sections of portions of the nucellar projection transfer cells at stages I (**A**), II (**B**), and III (**C**) of development. Tissue was triple-fixed sequentially with glutaraldehyde/paraformaldehyde, osmium tetroxide, and tannic acid (see Materials and methods). Note the abundance of mitochondria, rough endoplasmic reticulum and polyribosomes in the cytoplasm. Numerous multivesicular and paramural bodies (arrows) are located in close association with the wall ingrowths. Bars: 0.5 μm. *M* Mitochondrion; *Mu* multivesicular body; *Pa* paramural body; *Pr* polyribosomes; *Rer* rough endoplasmic reticulum; *Wi* wall ingrowths

Table 1. Plasma membrane amplification, surface areas, and potential sucrose fluxes of nucellar projection transfer cells in the developing wheat grain at 25 ± 3 days after anthesis

	% total nucellar projection cells[a]	Amplification	Plasma membrane surface area[b]		Potential sucrose flux[c]	
			− ingrowths	+ ingrowths	− ingrowths	+ ingrowths
Cells at stages of development						
Stage I	20.7 ± 1.8	3.84 ± 0.05	17	85	322	64
Stage II	13.7 ± 0.9	6.04 ± 0.07	11	418	498	11
Stage III	47.7 ± 1.3	6.91 ± 0.13	40	1902	140	3
Stage IV[d]	17.9 ± 1.2					
Nucellar epidermal cells	–	–	46	46	119	119
Total cells of nucellar projection	–	–	114	2451	48	2.2

[a] Values are means and standard errors of measurements from sections from 3 grains of 3 plants
[b] Plasma membrane surface area in 10^{-4} m^2
[c] Potential sucrose flux in 10^{-8} mol/m^2 plasma membrane/s
[d] No plasma membrane exists in the nucellar transfer cells at developmental stage IV

cumulation by the endosperm (and see Wang et al. 1994a).

The total flux was partitioned between nucellar projection cells at the three stages of transfer cell development and the nucellar epidermal cells using the total plasma membrane surface area offered by each cell type. Assuming that the plasma membranes of all the nucellar cells have an equal capacity for membrane transport of sucrose, the flux estimates indicate that cells at stage III of transfer cell development have spare transport capacity (Table 1). Cells at stage II could also accommodate the total rate of sucrose transfer, but those at stage I do not provide sufficient plasma membrane surface area to facilitate efflux to the endosperm cavity at observed rates of sucrose accumulation by the endosperm (Table 1).

Discussion

In this paper, we have presented micrographs of tissue fixed to either accentuate the features of the wall ingrowths (Figs. 2–6) or to provide the contrast required to resolve cytoplasmic characteristics (Fig. 7). The preservation of wall structure was excellent when tissue was fixed in a combination of glutaraldehyde, paraformaldehyde and tannic acid and post fixed in ferric chloride (method modified from Overall et al. 1982). On the other hand, sequential fixation with glutaraldehyde and paraformaldehyde, osmium tetroxide and finally tannic acid (method modified from Park et al. 1982) resulted in enhanced resolution of cytoplasmic features. Staining sections with potassium permanganate and lead citrate was found to complement these fixation procedures. The enhanced resolution of wall ingrowth and cytoplasmic features of the transfer cells offered by the use of these procedures has resulted in the opportunity to study the pattern of wall ingrowth formation in the nucellar projection of developing wheat grains. The wall ingrowth formation observed spans the phases from initial small ingrowths to highly complex compressed forms (Figs. 2–6). Further, in most systems such a sequence can only be visualized by selecting tissue at a range of developmental stages. For instance, development of epidermal transfer cells of cotyledons of *V. faba* (Offler in Bonnemain et al. 1991). In many species, the wall ingrowth differentiation stops short of becoming compressed. An example of this phenomenon is found in the thin-walled parenchyma transfer cells of the seed coat of *V. faba*. Their wall ingrowths are only papillate and become crushed by the expanding cotyledon before more extensive ingrowth differentiation can occur (Offler and Patrick 1993).

To our knowledge, the sequence of wall ingrowth differentiation exhibited in these four stages of transfer cell development has not been described previously. The descriptions of Cochrane and Duffus (1980) for barley nucellar projection transfer cells suggest a similar morphological sequence. However, the differentiation sequence from a papillate form (stage I) through

a process of increasing branching (antler-shaped ingrowths, stage I) and anastomosing to form a complex labyrinth (stage II) and then compression (stages III and IV) has not been described for a single tissue. The uniqueness of the system is not in the form of the ingrowths at the different stages of development, but in the coexistence of viable transfer cells exhibiting this range of wall ingrowth morphology. Morphological equivalents for papillate, antler-shaped and anastomosing wall ingrowths occur in other systems (e.g., seed coat transfer cells of *V. faba*, Offler and Patrick 1993; placenta pad transfer cells of the caryopsis of *Pappophorum subbulbosum*, Rost et al. 1984; and haustorium sporophyte transfer cells of *Funaria hygrometrica*, Browning and Gunning 1979, respectively). Further, the massive compressed wall ingrowths of the final stage of differentiation (stage III) are akin to the wall ingrowths of the epidermal transfer cells of the cotyledons of *V. faba* (Offler unpubl. data). However, in the case of these later cells, the inner border of the ingrowth wall remained irregularly and deeply lobed. Degeneration by infilling of cytoplasmic islets/interstices and crushing has been reported for a number of transfer cells (e.g., basal transfer cells of maize, Davis et al. 1990). Given the variability of morphology exhibited by the ingrowths (cf. Figs. 2–5), the question of classifying them as a single type of transfer cell arises. However, wall ingrowth differentiation is clearly sequential and transitional forms between "antler" and "compressed" ingrowths occur (Fig. 3 B). In addition, at earlier stages of grain development, the first formed ingrowths exhibit papillate and antler-shaped morphology and at later stages of grain development cells located in the equivalent position are characterized by massive ingrowths (Irwanto and Offler unpubl.).

A similar sequential differentiation of transfer cells from small to massive compressed ingrowths has been documented for the maize caryopsis (Davis et al. 1990). However, the finger-like ingrowths of these basal endosperm cells in maize are morphologically distinct from the ingrowths of the wheat transfer cells and their development is polarized (Davis et al. 1990). Interestingly, such polarization is a common feature of transfer cells formed in seed systems. For example, the aleurone transfer cells in barley (Cochrane and Duffus 1980) and the transfer cells of the seed coat and cotyledon of *V. faba* (Offler and Patrick 1993, Offler unpubl. data). The absence of polarization in these nucellar projection transfer cells may well indicate that sucrose is delivered at rates which ensure a relatively even sucrose concentration throughout the nucellar tissue (and see further on).

In general, the cytoplasmic characteristics of the nucellar projection transfer cells equate with those reported for other types of transfer cells (cf. Pate and Gunning 1972, Bonnemain et al. 1991). Comparison with other transfer cells of seed systems shows that only minor differences exist. For example, Davis et al. (1990) reported that the endoplasmic reticulum network of the basal endosperm cells of the maize caryopsis appears as long lengths distributed throughout the cytoplasm. The numerous paramural and multivesicular bodies found in association with the wall ingrowths and particularly evident at stages I and II of differentiation (Fig. 7 A, B; cf. Fig. 7 C), suggest rapid wall deposition, a function consistent with the continuing deposition of the wall ingrowths. Paramural bodies have been previously reported for transfer cells (Pate and Gunning 1972), and lomasomes are thought to have a role in wall formation by transferring polymers for wall deposition. Moreover, in soybean cotyledon cells (Grimes et al. 1992), the 62 kDa sucrose binding protein has been immunolocalized at the plasma membrane and high levels were associated with paramural bodies. Thus, the multivesicular and paramural bodies of the nucellar projection transfer cells may also contribute to their sucrose transport capacity.

In relation to the predicted role of these nucellar projection transfer cells as the principal cellular site for plasma membrane efflux of sucrose (Wang et al. 1994 a), the large numbers of mitochondria (Fig. 7) imply a high metabolic rate commensurate with active membrane transfer. Our previous studies (Wang et al. 1994 a) have demonstrated that the viable cells of the nucellar projection are interconnected by sufficient plasmodesmatal cross-sectional area (Figs. 2–4) to accomodate symplastic delivery of sucrose to the total plasma membrane surface area generated by the development of wall ingrowths. This plasma membrane surface area is amplified by 22 fold (Table 1). In other plant systems, for example, the seed coat (Offler and Patrick 1993) and cotyledons (Offler unpubl. data) of developing *V. faba* seed and the minor veins of *Pisum sativum* leaves (Wimmers and Turgeon 1991), morphological analysis and physiological studies have indicated that wall ingrowths of transfer cells could increase the capacity of the cells for solute transfer through increasing their plasma membrane surface areas. It is apparent that in the absence of wall ingrowth development there is insufficient plasma membrane to support observed rates of sucrose transport. Wall in-

growth development provides spare capacity, and it is significant that the fully differentiated stage III cells positioned proximally to the cavity alone have spare transport capacity. This suggests that there is a scope for regulatory increases in solute flow into the endosperm cavity.

Acknowledgements

H. L.W. thanks The University of Newcastle for a Postgraduate Research Scholarship. The research was supported by the Research Management Committee, The University of Newcastle.

References

Bonnemain JL, Bourquin S, Renault S, Offler CE, Fisher DG (1991) Transfer cells: structure and physiology. In: Bonnemain JL, Delrot S, Lucas WJ, Dainty J (eds) Recent advances in phloem transport and assimilate compartmentation. Ouest Editions, Paris, pp 74–83

Bray DF, Wagener EB (1978) A double staining technique for improved contrast of thin sections from Spurr-embedded tissue. Can J Bot 56: 129–132

Bremner PM, Rawson HM (1978) The weights of individual grains of the wheat ear in relation to their growth potential, the supply of assimilate and interaction between grain. Aust J Plant Physiol 5: 61–72

Browning AJ, Gunning BES (1979) Structure and function of transfer cells in the sporophyte haustorium of *Funaria hygrometrica* Hedw. J Exp Bot 30: 1233–1246

Chrispeels MJ (1980) The endoplasmic reticulum. In: Tolbert NE (ed) The biochemistry of plants, a comprehensive treatise, vol 1. Academic Press, New York, pp 389–412

Cochrane MP (1983) Morphology of the crease region in relation to assimilate uptake and water loss during caryopsis development in barley and wheat. Aust J Plant Physiol 10: 473–491

– Duffus CM (1980) The nucellar projection and modified aleurone in the crease region of developing caryopses of barley (*Hordeum vulgare* L. var. *distichum*). Protoplasma 103: 361–375

Davis RW, Smith JD, Cobb CB (1990) A light and electron microscope investigation of the transfer cell region of maize caryopses. Can J Bot 68: 471–479

Esau K, Cheadle VI, Gill RH (1966) Cytology of differentiating tracherary elements I. Organelles and membrane systems. Amer J Bot 53: 756–764

Felker FC, Shannon JC (1980) Movement of ^{14}C-labeled assimilates into kernels of *Zea mays* L. III. An anatomical examination and microautoradiographic study of assimilate transfer. Plant Physiol 65: 864–870

Grimes HD, Overvoorde PJ, Ripp K, Franceschi VR, Hitz WD (1992) A 62 kD sucrose binding protein is expressed and localized in tissues actively engaged in sucrose transport. Plant Cell 4: 1561–1574

Gunning BES (1977) Transfer cells and their roles in transport of solutes in plants. Sci Prog 64: 539–568

– Pate JS (1974) Transfer cells. In: Robards AW (eds) Dynamic aspects of plant ultrastructure. McGraw-Hill, London, pp 441–480

Jones MGK, Dropkin VH (1976) Scanning electron microscopy of nematode induced giant transfer cells. CytoBios 15: 58–59

Landsberg EC (1986) Function of rhizodermal transfer cells in the iron stress response mechanism of *Capsicum annuum*. Plant Physiol 82: 511–517

Lüttge U, Higinbotham N (1979) Transport in plants. Springer, Berlin Heidelberg New York

Maness MO, McBee GG (1986) Role of placental sac in endosperm carbohydrate import in *Sorghum bicolor* caryopses. Crop Sci 26: 1201–1207

Marchant R, Robards AW (1968) Membrane systems associated with the plasmalemma of plant cells. Ann Bot 32: 457–471

Newcomb W, Peterson RL (1979) The occurrence and ontogeny of transfer cells associated with lateral roots and root nodules in *Leguminosae*. Can J Bot 57: 2583–2602

Offler CE, Patrick JW (1993) Pathway of photosynthate transfer in the developing seed of *Vicia faba* L.: a structural assessment of the role of transfer cells in unloading from the seed coat. J Exp Bot 44: 711–724

– Nerlich SM, Patrick JW (1989) Pathway of photosynthate transfer in the developing seed of *Vicia faba* L. I. Transfer in relation to seed anatomy. J Exp Bot 40: 769–780

Overall RL, Wolfe J, Gunning BES (1982) Intercellular communication in *Azolla* roots: I. Ultrastructure of plasmodesmata. Protoplasma 111: 134–150

Park P, Yamamoto S, Kohmoto K, Otan H (1982) Comparative effects of fixation methods using tannic acid on contrast of stained and unstained sections from Spurr-embedded plant leaves. Can J Bot 60: 1769–1804

Pate JS, Gunning BES (1969) Vascular transfer cells in angiosperm leaves: a taxonomic and morphological survey. Protoplasma 68: 135–156

– – (1972) Transfer cells. Annu Rev Plant Physiol 23: 173–196

Rost TL, Lersten NR (1970) Transfer aleurone cells in *Setaria lutescens* (Graminae). Protoplasma 71: 403–408

– Izaguirre de Artucio P, Risley EB (1984) Transfer cells in the placental pad and caryopsis coat of *Pappophorum subbulbosum* Arech. (Poaceae). Amer J Bot 71: 948–957

Sofield I, Evans LT, Cook MG, Wardlaw IF (1977) Factors influencing the rate and duration of grain filling in wheat. Aust J Plant Physiol 4: 785–797

Spurr AR (1969) A low-viscosity epoxy resin embedding medium for electron microscopy. J Ultrastruct Res 26: 31–43

Tripathi S, Boulpaep E (1989) Mechanisms of water transport by epithelial cells. Q J Exp Physiol 74: 385–417

Wang HL, Patrick JW, Offler CE, Wardlaw IF (1993) A novel experimental system for studies of photosynthate transfer in the developing wheat grain. J Exp Bot 44: 1177–1184

– Offler CE, Patrick JW (1994 a) The cellular pathway of photosynthate transfer in the developing wheat grain. II. A structural analysis and histochemical studies of the transfer pathway from the crease phloem to the endosperm cavity. Plant Cell Environ (in press)

– – – Ugalde TD (1994 b) The cellular pathway of photosynthate transfer in the developing wheat grain. I. Delineation of a potential transfer pathway using fluorescent dyes. Plant Cell Environ 17: 257–266

Wimmers LE, Turgeon R (1991) Transfer cells and solute uptake in minor veins of *Pisum sativum* leaves. Planta 186: 2–12

Zees S, O'Bries TP (1971) Aleurone transfer cells and other structural features of the spikelet of millet. Aust J Biol Sci 24: 391–395